Case Studies in Thermal Engineering 72 (2025) 106325

Contents lists available at ScienceDirect

Case Studies in Thermal Engineering

journal homepage: www.elsevier.com/locate/csite

A concept for H_2-Diesel engines: CFD-driven dual spray optimization with energy/exergy analysis for enhanced performance and sustainable combustion

Kourosh Ghadamkheir [a], Mohammad Moghiman [a], Mohammad Hatami [b,*]

[a] Department of Mechanical Engineering, Ferdowsi University of Mashhad, Mashhad, Iran
[b] Department of Mechanical Engineering, Esfarayen University of Technology, Esfarayen, Iran

GRAPHICAL ABSTRACT

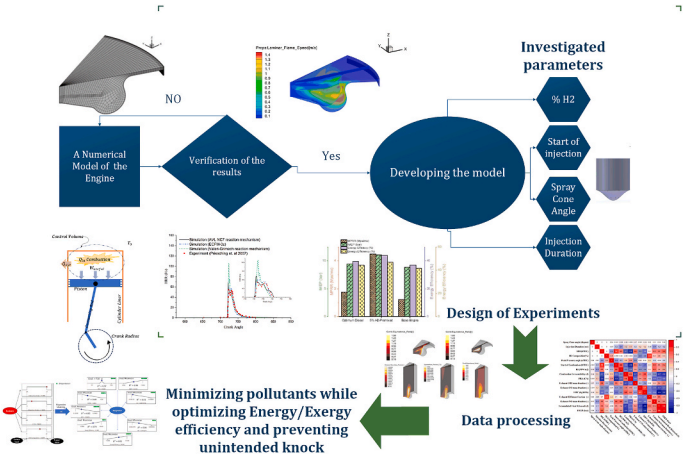

ARTICLE INFO

Keywords:
Energy/Exergy Analysis
Hydrogen
Emission Control

ABSTRACT

This study presents a comprehensive numerical investigation into the optimization of a dual-injection diesel engine fueled with diesel–hydrogen blends, aiming to enhance thermal performance while preventing severe knock. A detailed model was developed to assess the influence of key injection parameters on energy and exergy efficiencies, combustion characteristics, and output emissions. Knock occurrence was evaluated using ringing intensity and maximum pressure

* Corresponding author.
E-mail address: m.hatami@xjtu.edu.cn (M. Hatami).

https://doi.org/10.1016/j.csite.2025.106325
Received 28 December 2024; Received in revised form 22 April 2025; Accepted 12 May 2025
Available online 13 May 2025

Optimization
Knocking

rise rate as indicators. To ensure real-world applicability, datasets exceeding knock thresholds were excluded from the optimization process. Initial optimization of the baseline diesel engine resulted in a 2.61 % and 2.46 % increase in first- and second-law efficiencies, respectively. Introducing 5 % premixed hydrogen further improved these efficiencies to 5.1 % and 6.99 %, without surpassing knock limits. A dual-spray injection strategy was then implemented with varying hydrogen fractions. The optimal case with 20 % hydrogen achieved energy and exergy efficiencies of 44.68 % and 41.48 %, respectively, using specifically tuned injection parameters. While the spray cone angle had a smaller effect than the start of injection and injection duration, wider angles were more favorable for diesel-dominant diffusion combustion, whereas narrower angles enhanced premixed hydrogen combustion. Hydrogen injection improved combustion efficiency, reduced CO and CO_2 emissions, and lowered specific fuel consumption, albeit with increased nitrogen oxide and water vapor formation. Finally, a machine learning approach using computational dataset and regression-based optimization was developed to balance engine performance and emissions within knock-limited conditions, providing a practical route toward cleaner and more efficient hydrogen–diesel combustion engines.

Nomenclature

Acronym	Full name
BDC	Bottom Dead Center
CO	Carbon Monoxide
CO_2	Carbon Dioxide
CeO_2	Cerium Oxide
CI	Compression Ignition
DOE	Design of Experiments
ECFM-3z	Extended Coherent Flame Model - 3 zones
EGR	Exhaust Gas Recirculation
H_2	Hydrogen
H_2DI	Hydrogen-Direct Injected
H_2O	Water vapor
HCCI	Homogeneous Charge Compression Ignition
IMEP	Indicated Mean Effective Pressure
ISFC	Indicated Specific Fuel Consumption
ML	Machine Learning
MPRR	Maximum Pressure Rise Rate
MnO_2	Manganese Dioxide
NO_x	Nitrogen Oxides
PCCI	Premixed Charge Compression Ignition
PDE	Partial Differential Equation
PRA	Pressure Rise crank Angle (due to start of combustion)
PJB	Prosopis Juliflora Biodiesel
RCCI	Reactivity Controlled Compression Ignition
SOI	Start of Injection
TiO_2	Titanium Dioxide
TDC	Top Dead Center

Letters.

Letter	Description
A^q_{wall}	Exergy dissipated through heat transfer from the wall
ΔA_{sys}	Changes in the exergy of system
ΔU_{sys}	Changes in the internal energy of system
H	Enthalpy (J)
U	Internal energy (J)
S	Entropy (J/K)
ρ	Density (kg/m^3)
t	Time (s)
$\vec{u}$	Velocity vector (m/s)
ε	Vorticity dissipation rate (m^2/s^3)
k	Turbulent kinetic energy (m^2/s^2)
ζ	Turbulence frequency (−)
m_i	Mass of species i (kg)
W	Received work (J)
Q_{in}	Heat generated in the system due to combustion (J)
Q_{wall}	Heat dissipated from the cylinder wall (J)
S_{gen}	Generated entropy (J)

(*continued on next page*)

(*continued*)

Letter	Description
I	Destroyed exergy (J)
η_I	Energy efficiency (−)
η_{II}	Exergy efficiency (−)

1. Introduction

With the transportation sector contributing ~20 % of global GHG emissions and associated health impacts, manufacturers are increasingly implementing lean combustion technologies. However, these emission-reduction strategies frequently introduce trade-offs in engine performance characteristics [1,2]. Driven by environmental concerns and the depletion of fossil fuels, researchers are actively seeking sustainable and cleaner solutions. Recent research has explored sustainable alternatives to diesel fuel, including Prosopis juliflora biodiesel (PJB) blended with metal-based nanoparticles—cerium oxide (CeO_2), manganese dioxide (MnO_2), and titanium dioxide (TiO_2)—which can reduce engine exergy destruction by 3.5–6.4 % [3]. The growing urgency to address global fossil fuel dependence has positioned hydrogen as a promising alternative fuel for internal combustion engines. When applied in compression ignition engines, hydrogen demonstrates significant potential for reducing harmful emissions, including unburned hydrocarbons, carbon monoxide, carbon dioxide, and particulate matter [4]. As investigated by Karagoz et al., 2016 the diesel-enriched hydrogen could decrease the amount of CO and Smoke emissions by up to 69 % and 58 % respectively [5]. HCCI combustion regime for the hydrogen/n-heptane fuel would cause an increase of HC, while in a conventional system, it would reduce this particular emission [6,7]. Injecting HHO gas at a flow rate of 0.3 LPM in an RCCI combustion of a CI engine effectively reduces HC emission by 5.7 % and brake-specific fuel consumption by 4.58 %, though with an accompanying increase in nitrogen oxide emissions [8]. Dual-fuel injection systems, a novel technology for compression ignition engines, these injectors can simultaneously inject two different fuels. This capability can lead to significant improvements in engine performance, efficiency, and fuel consumption [9,10].

Exergy analysis serves as a powerful tool for diesel engine optimization, revealing pathways to reconcile competing objectives of performance enhancement, emission reduction, and fuel economy through thermodynamic system balancing [11,12]. A 3E (Energy, Exergy, Environmental) study of spirulina biodiesel and its diesel blends demonstrated significant effects in engine performance while reducing emissions by up to 28.09 % [13]. A study by Taghvifar et al. investigated the combined effects of hydrogen addition and turbocharging pressure ratio on a 1.8-L Ford direct injection diesel engine. They found that increasing the turbocharging pressure ratio led to a significant 14.7 kW improvement in power that enhances the exergy efficiency. However, the study also highlighted a potential drawback of premature hydrogen injection into the intake manifold. This can lead to faster combustion and a steeper rise in the temperature graph, ultimately increasing the risk of engine knocking [14].

Hydrogen's high flammability, often touted as an advantage for clean combustion, presents a potential challenge in CI engines. Unlike diesel fuel, hydrogen rapid combustion can lead to a sharp pressure rise rate within the cylinder, a phenomenon known as knock that is detrimental to engine performance and longevity, causing vibrations, increased wear, and potential engine damage [15,16]. Yao et al. [17] highlight this concern. They explore the concept of mixing ammonia with hydrogen to moderate the rapid flame propagation and mitigate knock in spark-ignition engines. Similar strategies are being explored for Compression ignition engines, aiming to leverage the benefits of hydrogen's clean combustion while addressing its knock propensity. Finding the optimal balance between the increased combustion efficiency provided by hydrogen and the prevention of extreme knocking in engines is a crucial area of research. This optimization process may involve adjusting injection parameters, such as timing and duration, exploring alternative injection strategies like dual or stratified injection systems, and potentially mixing hydrogen with other fuels that have lower flammability characteristics [18–20].

While hydrogen offers advantages such as high flammability, a low quenching distance, and a high flame speed, it also has a high auto-ignition temperature, which makes it somewhat resistant to auto-ignition. However, to store sufficient hydrogen in a vehicle for an acceptable travel range, a storage pressure of 700 bar is required, leading to significant logistical challenges [21–23]. A comprehensive understanding of fuel property interactions, fuel injection characteristics, and optimized valve timing enables researchers to develop advanced strategies for maximizing the efficiency of compression ignition engines [24,25]. Investigations by Ozkana et al. [26] revealed that employing multi-stage diesel fuel injection with varying injection start times to deliver a specific amount of fuel into the combustion chamber, as analyzed using a one-dimensional approach, demonstrated the potential impact of injection strategies on soot and nitrogen oxide emissions. Conversely, delaying the start of injection can lead to incomplete combustion, increased soot emissions, reduced thermal efficiency, and lower peak cylinder pressure. On the other hand, advancing the injection start timing by 9° in an ethanol-diesel blend engine can result in improved engine efficiency and increased peak pressure of up to 1 MPa compared to injection with a 3°_{CA} bTDC advance [27]. Also, injection duration plays a crucial role in the performance and emission characteristics of diesel engines, prompting extensive research into the effects of spray duration on these engines. Studies have demonstrated that both injection duration and start timing can significantly impact engine efficiency and exhaust emissions. When optimized, these parameters can enhance fuel atomization, improve air-fuel mixing, and increase combustion efficiency, ultimately leading to gains in engine torque and power output. A 2021 study found that reducing injection duration from 35°_{CA} to 15°_{CA} at a fixed injection start resulted in a 5.4 % increase in brake mean effective pressure and a decrease in specific fuel consumption [28].

Driven by environmental concerns and the depletion of fossil fuel resources, this study focuses on optimizing exergy in combustion engines to enhance efficiency and reduce pollution. Exergy analysis, which measures useable energy, is applied to improve fuel utilization and decrease greenhouse gas emissions. The research also simulates a novel dual-nozzle injector for diesel-hydrogen

combustion, investigating "ringing intensity" as a potential indicator for preventing extreme knock. Also, both premixed and direct injection of hydrogen are studied and compared with the baseline diesel engine. Additionally, machine learning techniques, specifically regression, are employed to optimize injection parameters, including fuel type, SOI, injection cone angle, and injection duration. This approach aims to balance first and second-law efficiencies while minimizing pollutants, fuel consumption, and the occurrence of engine knocking.

2. Materials and methods

The pre-processing stage of the computational fluid dynamics (CFD) solution involves defining boundary and initial conditions, which are presented below. A closed-cycle simulation strategy is employed for the engine simulation. This approach focuses on analyzing changes in fluid flow parameters within the cylinder during the intake valve closing (IVC) to exhaust valve opening (EVO) interval. As shown in Fig. 1, the compression ignition (CI) engine simulation employs a dual-injection mechanism of diesel fuel and gaseous hydrogen. To accurately capture the complex chemical reactions during combustion, two modeling approaches are employed: a detailed chemistry mechanism for comprehensive representation of the diesel-hydrogen mixture oxidation, and the computationally efficient ECFM-3z combustion model for large-scale simulations.

2.1. Theoritical background

Generally, studying the behavior of fluid flow in any physical system requires first identifying the governing equations, which are predominantly partial differential equations (PDEs), and then solving them using analytical or numerical methods to gain a proper understanding of the fluid motion. In this research, the focus is on a sector of a complete piston from a direct injection diesel engine. Due to the closed nature of the simulation cycle, only the compression and power cycles will be modeled, and the open cycle modeling will be omitted due to high computational time and volume.

In the above modeling, the equations governing the flow inside the cylinder include the conservation of momentum, mass, energy, and species, which will be discussed in detail in the following sections [29].

$$\frac{\partial \rho}{\partial t} + \nabla \cdot (\rho u) = 0 \tag{1}$$

In equation (1), the term $\partial\rho/\partial t$ represents changes in fluid density over time. This is crucial in combustion engines where the cylinder and piston undergo compression, affecting the compressible fluid's density. The ideal gas state equation models this time-varying density. Additionally, the term $\nabla\cdot(\rho u)$ expresses the divergence of the flow velocity vector within the computational domain. In addition to the above equation, conservation of momentum, which relates the rate of momentum in a control volume to the net forces acting on it, is another equation that must be solved, and its mathematical expression is as follows.

$$\frac{\partial(\rho u_i)}{\partial t} + \frac{\partial(\rho u_i u_j)}{\partial x_j} = -\frac{\partial P}{\partial x_i} + \frac{\partial}{\partial x_j}\left(\mu\left(\frac{\partial u_i}{\partial x_j} + \frac{\partial u_j}{\partial x_i} - \frac{2}{3}\frac{\partial u_k}{\partial x_k}\delta_{ij}\right)\right) + \frac{\partial}{\partial x_j}\left(-\rho\overline{\acute{u}_i\acute{u}_j}\right) \tag{2}$$

In this context, u denotes the velocity vector with three components. The δ_{ij} denotes the Kronecker delta operator, and $\overline{\acute{u}_i\acute{u}_j}$ represents the Reynolds stress tensor.

In this study, the Boussinesq approach, detailed in equation (3), was employed. Initially, the eddy viscosity was computed using the k-ζ-f model. By incorporating the turbulence stress term (which is linked to eddy viscosity through the Boussinesq equation) into the momentum equation, the fluid flow problem can be solved [30].

$$-\rho\overline{\acute{u}_i\acute{u}_j} = 2\mu_t S_{ij} - \frac{2}{3}\rho k\delta_{ij} \tag{3}$$

To describe the state of chemical reactions in the combustion chamber and control the kinetics of the reaction, species transport equation must be solved. In fact, by using the species equation, the mass distribution and penetration rate of any chemical species in the fluid are determined. Equation (4) describes the general form of the species transport equation [31].

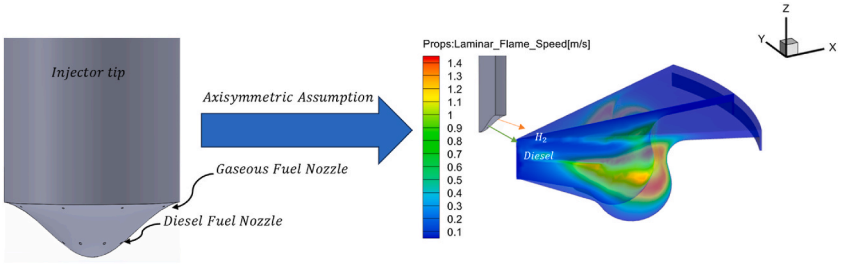

Fig. 1. Schematic view of dual-channel injector tip and the modeled engine segment.

$$\frac{\partial}{\partial t}(\rho Y_k)+\frac{\partial}{\partial x_i}(\rho u_i Y_k)=\frac{\partial}{\partial x_i}\left(\left(\rho D+\frac{\mu_t}{Sc_t}\right)\frac{\partial Y_k}{\partial x_i}\right)+S_{y_k}\quad k=1,2.....,species \tag{4}$$

In the above equations, Y_k is equal to the species mass fraction, u_i is the velocity, D is the diffusion coefficient, Sc_t is the Turbulent Schmidt number, which has a value of about 0.7, and S_{y_k} is the source term caused by the production or consumption of the species shown in equation (5).

$$S_{y_k}=\dot{R}_k.M_k \tag{5}$$

which in this equation $\dot{R}_k$ is equal to the rate of production or consumption of the kth species and M_k is the molar mass of the specific species.

2.2. Combustion modeling

In this study, combustion simulations were conducted using two methods to compute the energy equation's reactive term. Initially, the coupling of a chemical mechanism with CFD software enabled the retrieval of equilibrium constants and stoichiometric coefficients for each reaction from the Valeri and Grimech3.0 mechanisms developed by Rahimi et al. [32]. This approach enabled the real-time calculation of species production and consumption rates based on kinetic reaction relationships. The decision to use Grimech 3.0 along with Valeri was driven by the requirement to model hydrogen oxidation, which is not included in Valeri mechanism. Furthermore, the AVL NC7 mechanism from AVL GmbH was employed for engine diffusion combustion, despite its closed-source nature in the AVL Fire software [33,34]. The combustion process initiates upon reaching predefined pressure and temperature conditions, triggering fuel decomposition and subsequent reaction rate calculations. This detailed approach, while time-intensive, is essential for studying intermediate radicals and conventional pollutants in combustion modeling. Hence, after comparing numerical results, the accuracy of both reaction mechanisms and the combustion model has been investigated.

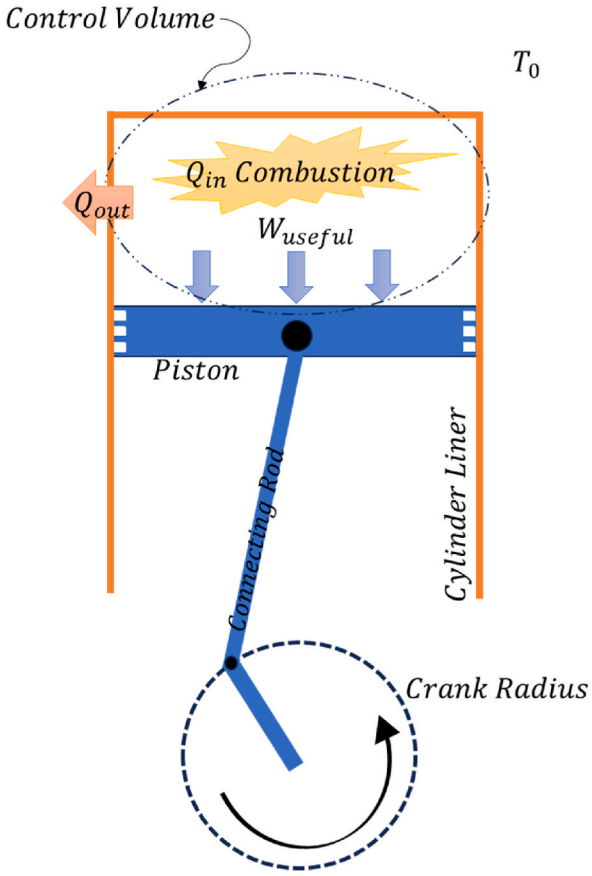

Fig. 2. Combustion chamber control volume.

2.3. Thermodynamic modeling

To model the first law of thermodynamics, a control volume similar to the schematic shown in Fig. 2 was employed. This control volume captures the system's initial condition (after closing of intake valve) with air inside, and progresses through compression and heat generation from combustion to reach final conditions (before exhaust valve opening).

Within this thermodynamic framework, energy and exergy transfers from the cylinder wall, along with the amount of useful work in each cycle, are modeled and quantified. The energy balance equation is expressed mathematically as follows [35]:

$$Q_{cv} - W_{cv} = \Delta U_{sys} \tag{6}$$

The change in internal energy (ΔU_{sys}) spans from closing the air valve to opening the exhaust valve. Heat generated by combustion typically increases final internal energy, as combustion gases hold more thermal energy than incoming air. This energy difference corresponds to the heat released into the atmosphere through exhaust [36]. Q_{cv} represents net heat gained due to combustion, while W_{cv} denotes total useful work done by the system. The first law efficiency, a key focus of this study, is defined as equation (7):

$$\eta_{\mathrm{I}} = \frac{W_{cv}}{Q_{in}} = \frac{\int_{cv} P.dv}{m_{Diesel\ burnt}.LHV_{Diesel} + m_{H2\ burnt}.LHV_{H2}} \tag{7}$$

where P is the pressure, dv is the displacement volume, m_{burnt} is the amount of fuel burned and LHV is the heating value of each of the used fuels. But in order for the potential state of the system to be checked and for the efficiency to be estimated along with the quality of the energies converted to each other, the second law is needed, which is mathematically expressed in equation (8) as follows [37].

$$\frac{Q}{\mathrm{T}_0} \leq \Delta S \rightarrow \frac{Q_{wall}}{\mathrm{T}_0} + S_{gen} = S_2 - S_1 \tag{8}$$

In the above context, ΔS represents the entropy changes of the system, while S_{gen} quantifies the generated entropy. Q_{wall} denotes the heat exchanged from the system to the environment at temperature T_0, typically ambient temperature. However, in combustion engines, calculating the system's exergy efficiency is crucial [38]. To achieve this, the first step is to compute S_{gen}, which is then multiplied by the ambient temperature to determine the destroyed exergy amount. Equation (9) mathematically expresses the exergy balance required for second-law thermodynamic analysis [39].

$$\Delta A = \mathrm{Ex}_{\mathrm{f,ch}} + m_{in}\mathrm{b}_{in} - m_{out}\mathrm{b}_{out} - \mathrm{Ex}_W - \mathrm{Ex}_Q - \mathrm{I} \tag{9}$$

where, I denotes the exergy destroyed by combustion, Ex_Q represents exergy lost through heat transfer from the wall, and Ex_W signifies work exergy. Additionally, $m_{in}\mathrm{b}_{in}$ denotes the exergy of the incoming flow from the air valve (initial state), while $m_{out}\mathrm{b}_{out}$ represents the exergy of the flow exiting from the smoke valve (final state). The reversible work, $\mathrm{Ex}_{\mathrm{f,ch}}$, equates to the chemical exergy of the fuel in this study. ΔA denotes the term encompassing exergy changes in the system, incorporating thermomechanical and chemical exergy components.

But the efficiency of the second law, which is the amount of available exergy received (W_{cv}) to the total exergy entered into the system (A_{ch}), is mathematically expressed in equation (10) as follows [40]:

$$\eta_{II} = \frac{W_{cv}}{\mathrm{Ex}_{\mathrm{f,ch}}} = \frac{\int_{cv} P.dv}{m_{Diesel}.A_{ch,Diesel} + m_{H_2}.A_{ch,H2}} \tag{10}$$

2.4. CFD modeling

The engine used for this numerical modeling was a conventional diesel engine that its specifications are illustrated in Table .1.

Table .2 displays all numerical models utilized for simulating flow turbulence motion, fuel combustion and evaporation, and emission analysis.

Table 1
Engine specification.

Bore	85 mm
Stroke	94 mm
Displacement	533.4 cm^3
Bowl shape	Omega
Connecting rod length	161 mm
Number of injection holes	8
Compression ratio	16:1
Aspiration	TCI

Table 2
Numerical models used in the simulation.

Module	Simulation methodology
Combustion model	Reaction mechanisms / ECFM 3-z
Spray evaporation model	Multi component
Discretization method	Simple
Turbulence model	k-ζ-f
Particle interaction model	Schmit
Breakup model	Wave
Nitrogen oxides formation	Zeldovich
Engine knocking	J. A. Eng equation[1] [41]

2.5. Model validation

In this research, two methods were used for combustion modeling: the ECFM-3z combustion model and a chemical mechanism. Pressure and heat release rates from simulations were compared with experimental data achieved on the base engine with injection systrm of "BOSCH Piezo CR", "spray angle of 158°", "injection pressure between 1200 and 1600 bar", and "IMEP equal to 8.3 bar" by Priesching et al. [42]. Using the ECFM-3z model, the difference in maximum pressures was minimal, within 4 %. The AVL NC7 mechanism showed approximately 4 % deviation, while the Valeri-Grimech 3.0 combination by Rahimi et al. exhibited up to 14.5 % variance in maximum pressures. Diesel combustion, characterized by two-stage combustion, was accurately simulated by the ECFM-3z model, showing two distinct heat release peaks (Fig. 3). Based on these findings, the ECFM-3z model was chosen for further simulations due to acceptable accuracy and extensive less calculation time.

To ensure simulation accuracy, the results were compared with experimental data. Table .3 outlines the initial and boundary conditions established for this numerical study.

A grid independence analysis was performed to ensure that the numerical results are not affected by the mesh size, as illustrated in Fig. 4. It was found that variations in the results became minimal when the cell sizes were below 2 mm, confirming that this model meets convergence requirements with reasonable accuracy.

By selecting a grid size of 1 mm and setting two boundary layer mesh layers at 0.1 mm, the local and average changes of y + are shown in Fig. 5. Due to the curved surfaces and varying flame behavior within the combustion chamber, y + changes more in turbulent areas and less around the flame, especially near the top dead center. The y + values for the engine with asymmetric geometry are below 35, indicating acceptable accuracy near the wall in this study.

3. Results and discussion

In this section, the numerical results of combustion modeling for the base single-injection diesel engine and the modified hydrogen-fueled dual-injection engine are discussed. The studied parameters in this research have been listed in Table .4.

3.1. Diesel engine simulation

One advantage of transient CFD modeling is its ability to capture instantaneous interactions in the combustion chamber, eliminating the need for fast imaging facilities to estimate flame propagation. As illustrated in Fig. 6, the propagation of the diesel combustion flame initiates near top dead center (TDC), consistent with expected ignition timing under conventional operating conditions. Notably, the simulation reveals a significant accumulation of unburnt fuel within the piston bowl region upon exhaust valve opening (EVO). This observation suggests incomplete combustion, likely attributable to localized fuel-rich zones or insufficient mixing prior to flame quenching.

After the simulations were conducted by varying one of the levels of the studied inputs, an experiment matrix was designed to

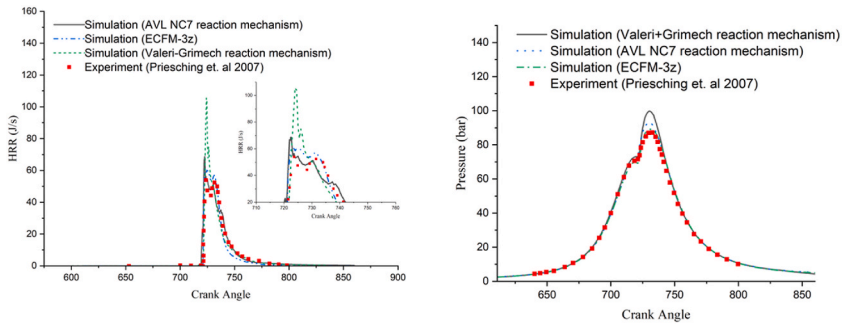

Fig. 3. Pressure and HRR diagrams comparison in simulation and experimental data.

Table 3
Initial and boundary conditions of the base model.

Start of injection timing	7.5° bTDC
Intake valve closed	110° bTDC
Exhaust valve opened	140° aTDC
Pressure at IVC	2.495 bar
Temperature at IVC	422.5 K
Liquid temperature	365 K
Turbulent kinetic energy	35 m^2/s^2
Dissipation rate	6804.78 $\frac{m^2}{s^3}$
Cylinder Head	Fixed Wall - Temperature 550.15K
Piston	Wall with movement - Temperature 575.15K
Liner	Wall with movement - Temperature 475.15 K
Axis	Symmetry
Segment cut	Periodic inlet/outlet

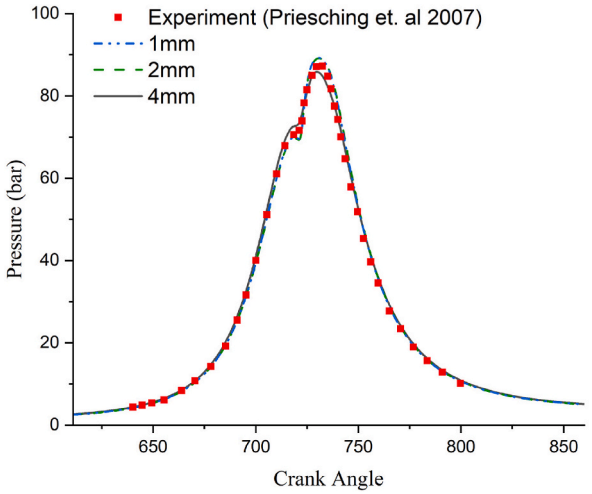

Fig. 4. grid independency analysis with pressure diagram.

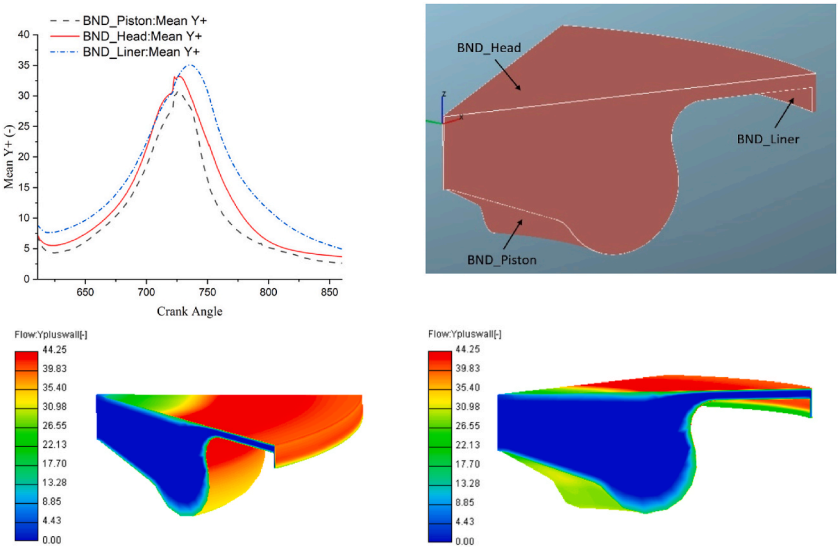

Fig. 5. Local and mean amount of calculated y+ in simulated segment.

Table 4
Studied parameters whith their simulated range.

% H_2	0 %, 5 %, 10 %, 20 %
Spray Cone angle	3.75, 7.875, 12
Start of injection	25 bTDC, 15 bTDC, 5 bTDC
Injection duration	1.2 ms, 1.6 ms, 2 ms

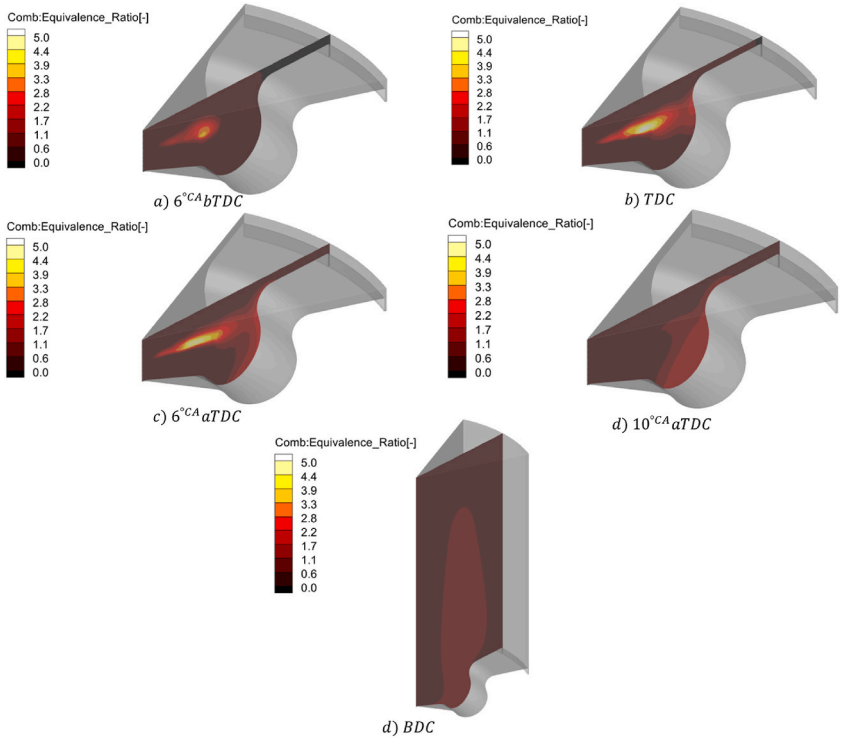

Fig. 6. Local distribution equivalance ratio of the balinese diesel engine at various crank angles.

investigate the simultaneous effects of modifying engine injection parameters on efficiency and performance. The results of these simulations, where each parameter (SOI, injection duration, and spray cone angle) was analyzed at 3 levels, can be found in the table included in Appendix I.

As illustrated in Fig. 7, the influence of baseline diesel engine spray parameters on combustion performance was systematically evaluated. Among the variables examined—spray cone angle, injection duration, and start of injection (SOI)—the spray cone angle exhibited the least pronounced effect on in-cylinder pressure variation. However, the results indicate that a wider cone angle enhances air-fuel mixing efficiency, leading to a significant reduction in carbon monoxide (CO) emissions by up to 62.14 %. This improvement can be attributed to improved fuel dispersion and subsequent oxidation due to greater interaction with ambient air.

Furthermore, reducing the injection duration was found to elevate peak in-cylinder pressure while simultaneously decreasing CO emissions. This trend suggests that shorter injection events promote more rapid and complete combustion, minimizing the formation of partial combustion products.

The start of injection (SOI) has become an important factor influencing engine performance. When injection occurs much earlier than top dead center (TDC), it can cause excessive pressure rise rates, leading to mechanical stress and potential engine damage. On the other hand, significantly retarded combustion results in lower thermal efficiency due to late heat release, which increases the chances of misfires and incomplete combustion.

The base engine simulations with pure fuel analyzed knocking potential, energy efficiency, exergy, and pressure rise due to combustion (PRA). Optimizing diesel injection timing and shortening spray duration enhanced first and second law efficiencies, increasing IMEP. However, cases with high RI and PRR far from 720° were deemed impractical due to the risk of engine damage. Premature combustion increased cylinder temperatures, creating thermal management challenges. While advancing injection timing enhanced engine performance theoretically, very early injection (25° bTDC) combined with a short injection duration led to premature ignition, significantly increasing the risk of knock. Optimization at SOI 15° bTDC, injection duration 1.6 ms, and spray cone angle 12° maximized efficiencies, achieving 24.15 % CO reduction, and improved mechanical work output as shown in Fig. 8. In this condition, first and second law efficiencies reached 44.24 % and 39.54 %, respectively.

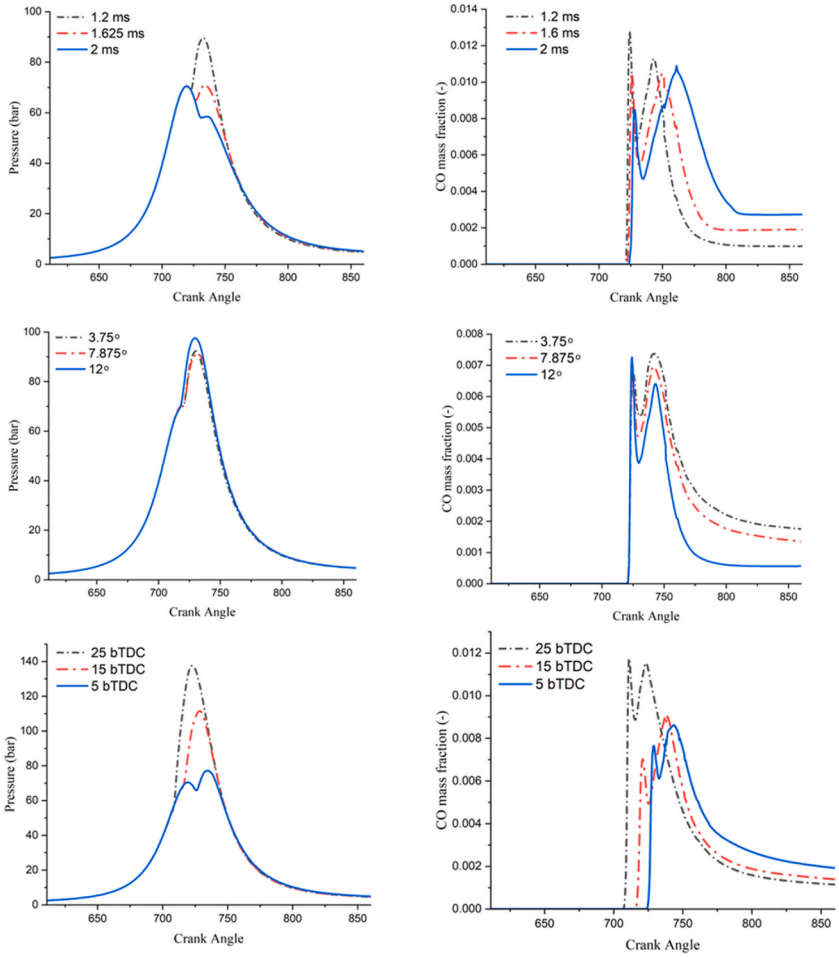

Fig. 7. In-cylinder pressure and the CO emission variation under different simulated injection strategies.

3.2. Diesel/hydrogen-fueled engine

In order to study hydrogen combustion effects more deeply, two approaches have been used to do so. The first one is to simulate the hydrogen in a homogeneous blend injected from the intake port, and then diesel is directly injected into the combustion chamber as the high-reactive fuel and the starter of combustion. While the second approach is to use a dual-nozzle direct injection mechanism to model both diesel and hydrogen being mixed and sprayed directly.

3.2.1. Premixed hydrogen addition

The simulation led to the fact that due to a very high flammability and low ignition energy, hydrogen can be combusted easily. As illustrated in Fig. 9, for cases where the amount of premixed hydrogen would be 10 or 20 %, the pressure rise rate will exceed its standard value and would not be favorable in real-world engine conditions. Hence, the 5 % hydrogen was chosen to be simulated as the port injected fuel.

In this case, the calculated ringing intensity was about 1.35, and the maximum pressure rise rate (MPRR) was approximately 4.46. Compared to the premixed hydrogen cases, this indicates a much smoother combustion process. As shown in Fig. 10, both the first- and second-law efficiencies were optimized, reaching 46.73 % and 44.07 %, respectively. Additionally, due to more rapid combustion, energy was converted to mechanical work at a more optimal crank angle, resulting in an increase in IMEP in the presence of hydrogen.

3.2.2. Direct-injection hydrogen addition

As mentioned, the second approach involves using two nozzles within the combustion chamber: one nozzle to inject diesel at 3.5 mm from the top dead center and another to inject hydrogen at 1.5 mm from the top dead center. This method has been utilized to continue simulations and optimize performance of the engine. Hydrogen is injected into the combustion chamber simultaneously with the base fuel. This approach prevents the accumulation of hydrogen inside the chamber and helps control its sudden combustion by enabling gradual spraying along with the diesel fuel.

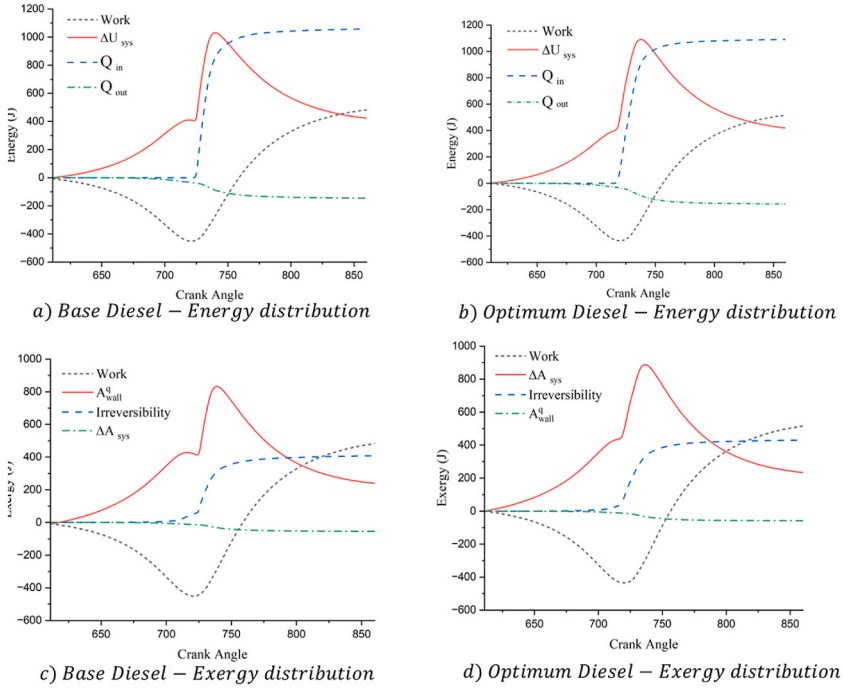

Fig. 8. Energy/Exergy distribution in base and optimized diesl engines.

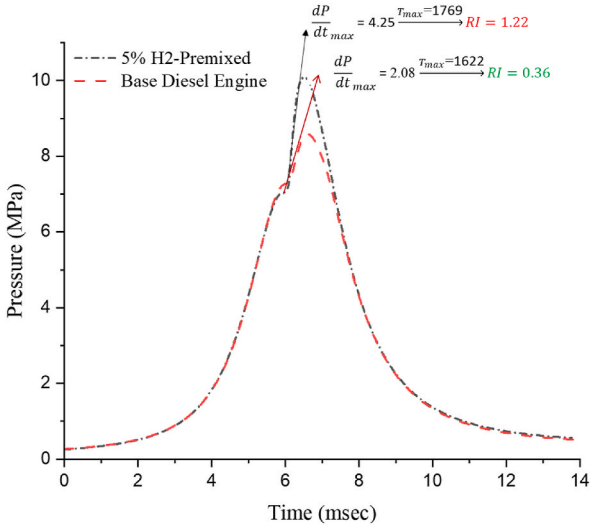

Fig. 9. Pressure variation under different H_2 mass being injected.

As shown in Fig. 11, the local equivalence ratio in flame regions for 20 % hydrogen spray near the injected fuel is higher than the other sides of the cylinder due to hydrogen's gaseous nature, molecular energy, and higher flame speed. Optimizing the single-fueled diesel engine by advancing injection timing and controlling injection rate improves efficiency and reduces emissions, but increases knocking potential. Also, Direct hydrogen injection into the combustion chamber requires a complex experiment matrix to optimize diesel flame timing and hydrogen ignition. Both fuels share the same start and duration of spraying for simultaneous combustion. This method aims to achieve maximum first and second law efficiency while managing knocking potential.

To refine the analysis, simulation cases exceeding standard knocking criteria, specifically those with a pressure rise angle (PRA) greater than 1°CA before top dead center, were excluded from consideration. Fig. 12 presents the first- and second-law efficiencies, along with the average effective pressure, across the remaining simulated cases. The optimal operating conditions were identified as follows: Run ID #51 for pure diesel combustion, Run ID #69 for 10 % hydrogen direct injection, and Run ID #28 for 20 % hydrogen direct injection. As demonstrated in Fig. 12, the 20 % H_2DI case exhibited a significant enhancement in both engine performance and

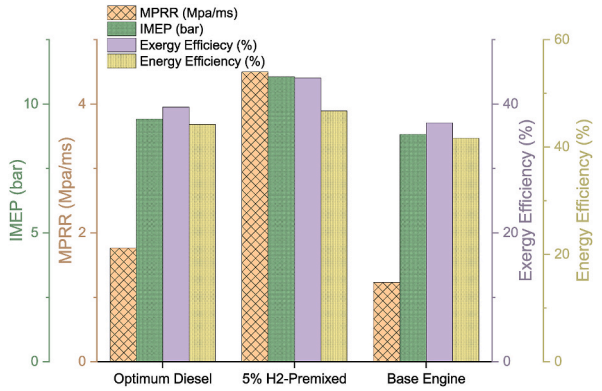

Fig. 10. Pressure variation under different H_2 mass being injected.

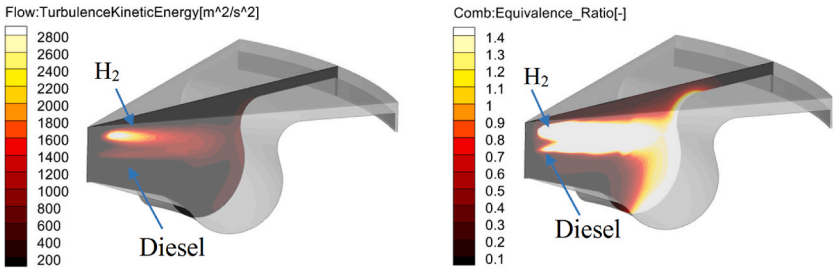

Fig. 11. Local Turbulent kinetic energy and equivalance ratio of the dual injection H2-Diesel engine at TDC.

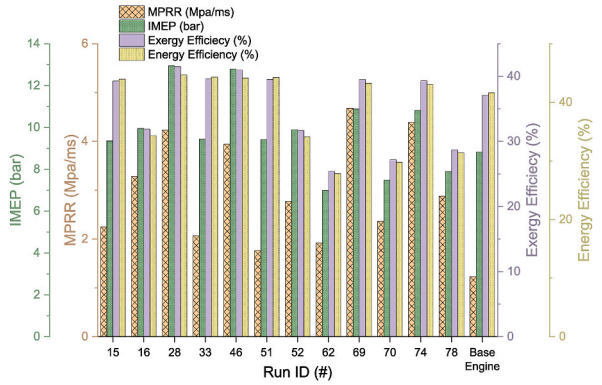

Fig. 12. Performance and efficiencies of standard cases with allowable knocking index.

thermodynamic efficiency compared to the baseline diesel configuration, while maintaining minimal knocking propensity.

As observed in Fig. 13, increasing hydrogen content in the fuel elevates cylinder temperatures alongside pressure. These parameters enhance performance in hydrogen-enriched engines, as indicated by calculations in this study. Hydrogen fractions of 10 % and 20 %, under specified diesel injection conditions, can expand the enclosed area in the pressure-volume diagram which leads to higher engineperformance.

Fig. 14 shows that with the effective use of hydrogen in the engine, it is possible to contribute to the relative reduction of carbon pollutants; Because the main product of hydrogen combustion is water vapor, it is expected that by increasing the percentage of hydrogen in the fuel being consumed and decreasing the share of heavy fuel, H_2O vapor will be added to the exhaust composition and carbon dioxide as a greenhouse gas be reduced up to 20.06 % for the optimum 20 % H_2DI case.

Fig. 15 illustrates that as efficiency improves and combustion temperatures rise, carbon monoxide emissions are significantly reduced, while nitrogen oxides levels increase. In fact, enhancing the second law efficiency improves the interactions within the system, leading to the extraction of more useful work. This also minimizes pollutants generated by incomplete combustion, which are negative impacts of the system on the environment.

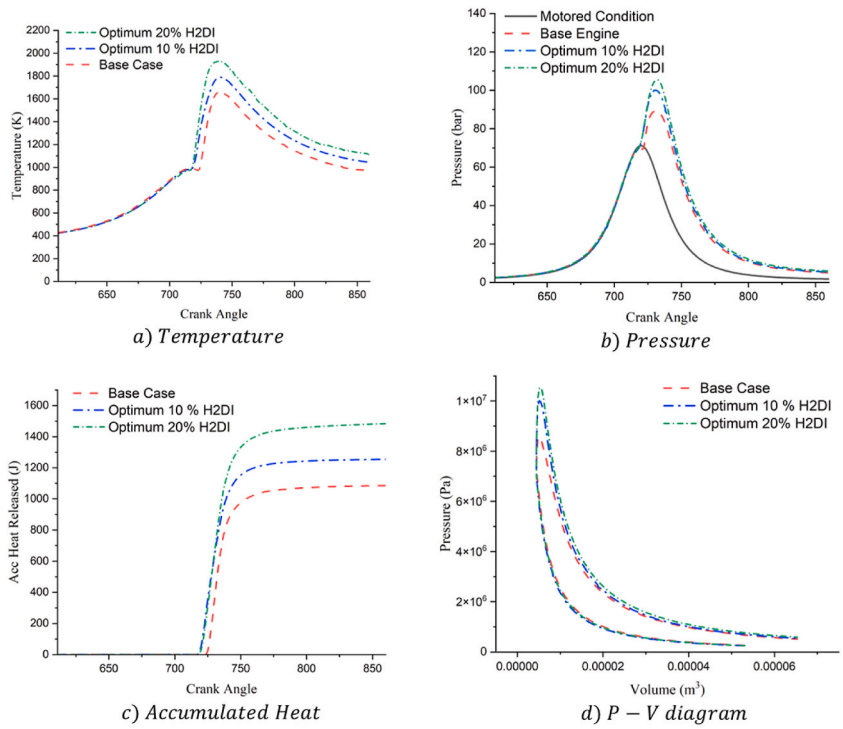

Fig. 13. Performance and efficiencies of standard cases with acceptable knock index.

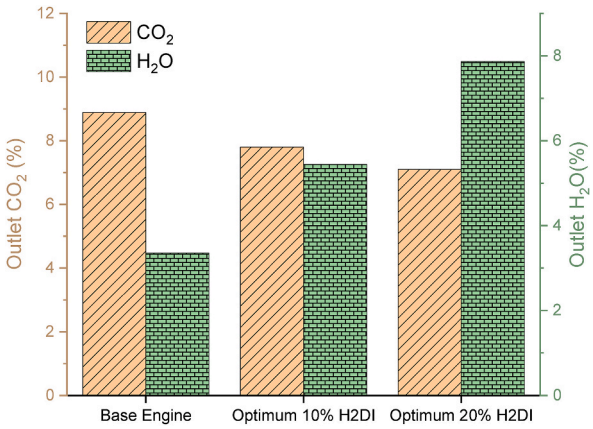

Fig. 14. Performance and efficiencies of standard cases with acceptable knock index.

3.3. Multi-objective optimization and correlation analysis

The Kendall correlation analysis shown in Fig. 16 indicates that the spray cone angle has the least impact on engine performance, as evidenced by its correlation coefficient being close to zero compared to the three other parameters examined. The analysis also clarifies the relationships among the input and output variables. Coefficients close to $+1$ or -1 indicate strongly aligned or inversely related effects, respectively, while values near zero suggest minimal influence between the pairs.

A significant finding is the negative correlation of -0.4 between hydrogen enrichment and indicated specific fuel consumption, highlighting how hydrogen can improve combustion efficiency. However, this advantage comes with increased emissions of water vapor and nitrogen oxides, which is consistent with the higher adiabatic flame temperature and oxidative potential of hydrogen-blended combustion. Furthermore, the analysis reveals an inverse relationship between thermodynamic irreversibility and the indicated mean effective pressure. This suggests that by reducing irreversibility, thus maximizing energy extraction from the fuel, it is possible to enhance the usefulwork output of the engine.

Optimizing engine performance necessitates a robust statistical modeling framework to establish responses as functions of critical

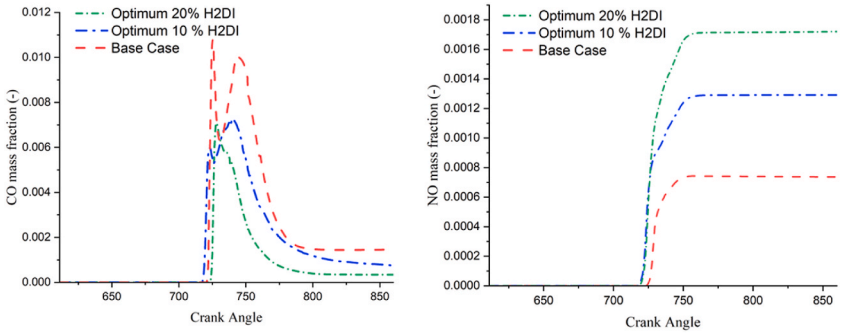

Fig. 15. Performance and efficiencies of standard H_2-Diesel cases with acceptable knock index.

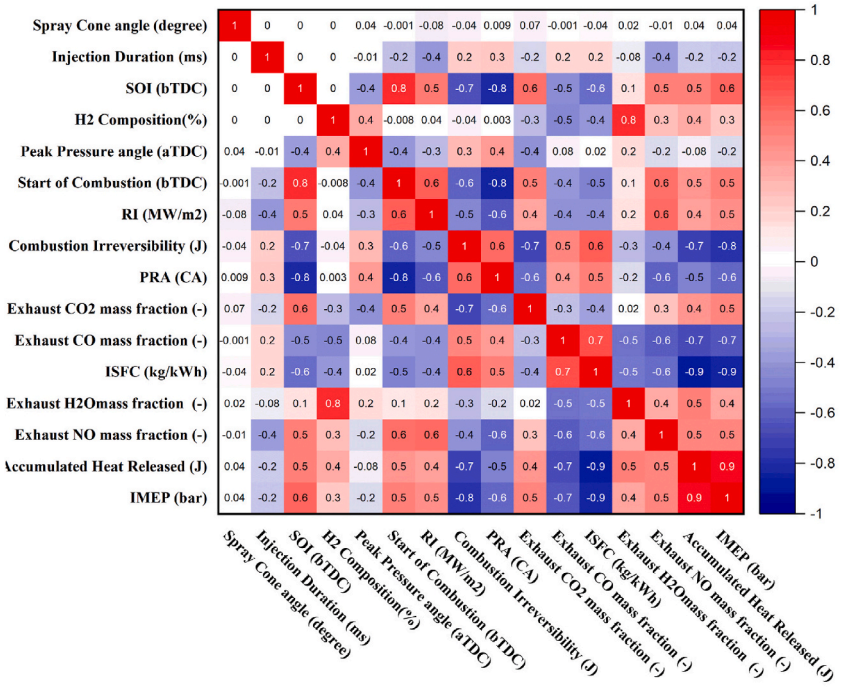

Fig. 16. Correlation matrix between input and output investigated parameters.

input variables, ensuring that operational constraints and objective functions are systematically defined. In this study, response levels and parameter boundaries were derived from CFD simulations guided by a design of experiments (DoE) approach. The trained regression model, developed using Design Expert software (Fig. 17), was employed to maximize first- and second-law thermodynamic efficiencies while simultaneously minimizing pollutant emissions and fuel consumption.

The optimization results indicate that the following parameters yield optimal performance: an injection duration of 1.39 ms, a spray cone angle of 11.99°, and a start of injection (SOI) timing of 11.12° bTDC. Furthermore, the model recommends a hydrogen enrichment level of 13.26 %, which is projected to achieve an energy efficiency of 41.44 % and an exergy efficiency of 38.02 %. To mitigate knocking, the peak pressure rise rate must be constrained below 5 MPa/ms, aligning with established engine durability thresholds. Additionally, the optimization framework prioritizes the reduction of carbon monoxide, and nitrogen oxides, alongside minimizing indicated specific fuel consumption ISFC to enhance both environmental and operational performance.

The optimization framework leverages a defined objective function to identify an optimal solution space. For the specific investigated engine, response parameters are derived through multivariable regression modeling as explicit functions of input variables (e.g., SOI, injection duration, cone angle, and hydrogen ratio).

Given the study's focus on quantifying energy and exergy efficiency, the regression-derived surrogate model circumvents the need for computationally intensive thermodynamic simulations. Specifically, the model directly outputs efficiency values as functions of spray cone angle, injection duration, hydrogen fuel composition, and start of injection timing, while concurrently enforcing

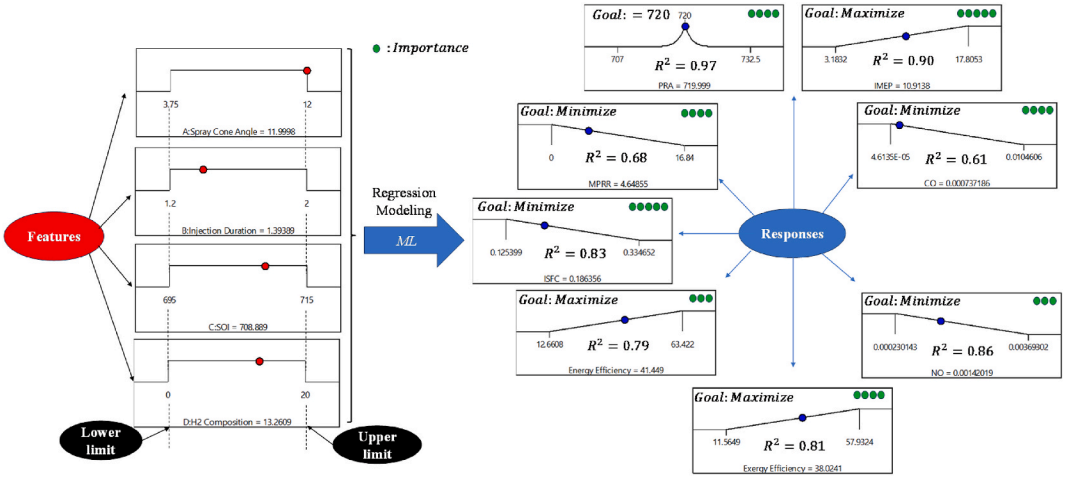

Fig. 17. Performance and efficiencies of standard cases with acceptable knock index.

combustion stability constraints such as maximum pressure rise rate. The analytical relationships governing these outputs are provided in Appendix II. This approach enables rapid prediction of system performance while ensuring adherence to knock mitigation criteria (MPRR <5 MPa/ms) and emission reduction targets.

4. Conclusion

This study examines critical injection parameters in compression ignition engines through detailed modeling and multi-objective optimization. The analysis assesses both energy and exergy efficiencies while considering emission characteristics. Key findings are summarized as follows.

- The use of hydrogen as a supplement to primary fossil fuels reduces carbon monoxide and carbon dioxide emissions in the combustion engine.
- In single-fuel diesel operation, employing a wider spray cone angle (12°) increases nitrogen oxide emissions while reducing carbon monoxide. This configuration enhances air-fuel mixing, resulting in a 14 % higher heat release rate peak during the diesel second combustion phase.
- Optimizing the primary engine without hydrogen shows that increasing injection duration with a 7.5-degree advance in SOI achieves energy efficiency of 44.24 % and exergy efficiency of 39.54 %.
- The limiting factor for injection timing and duration is allowable knock, calculated by ringing intensity. A very advanced start of injection increases knocking, causing potential engine damage.
- Using 5 % premixed hydrogen achieves 46.73 % energy efficiency and 44.07 % exergy efficiency while keeping ringing intensity below 2 MW/m^2.
- Direct hydrogen injection at 20 % mass fraction with extended injection duration (1.6 ms) and 15° advanced timing demonstrates significant performance improvements, increasing mechanical useful work by 47.72 % and enhancing exergy recovery compared to baseline diesel operation.
- Correlation analysis demonstrates that increased exergy efficiency reduces CO emissions while improving the system's thermodynamic performance, consequently reducing specific fuel consumption. Results indicate that hydrogen enrichment, start of injection timing, and injection duration have significantly greater influence than spray cone angle on combustion characteristics.
- Multi-objective regression optimization identifies an optimal hydrogen-enriched combustion configuration: a 13.26 % H_2 mass fraction, 1.39 ms injection duration, an 11.99° spray cone angle, and an 11.12° bTDC start of injection. This configuration simultaneously reduces CO emissions while decreasing fuel consumption and increasing indicated mean effective pressure compared to conventional operation.

As demonstrated, hydrogen application in combustion engines could effectively reduce carbon emissions. Through fine-tuning of injection parameters using regression-based and statistical analysis, an optimal system configuration was identified that improves performance while maintaining knocking within allowable limits. Future research should investigate additional carbon-neutral fuel blends, particularly hydrogen-ammonia mixtures in combination with e-fuels such as oxymethylene ethers, to achieve comprehensive improvements in: emission reduction, engine performance, and knocking mitigation.

CRediT authorship contribution statement

Kourosh Ghadamkheir: Software, Methodology. **Mohammad Moghiman:** Investigation, Formal analysis. **Mohammad Hatami:** Validation, Supervision.

Declaration of competing interest

The authors declare that they have no known competing financial interests or personal relationships that could have appeared to influence the work reported in this paper.

Appendix I

Table 1
Simulation matrix for parametric analysis of hydrogen-enriched combustion with variable injection parameters

ID	Spray Cone Angle (degree)	Injection Duration (ms)	SOI (CA)	H_2 (%)	RI (MW/m^2)	PRA (CA)	IMEP (bar)	Exergy Efficiecy (%)	Energy Efficiency (%)
1	3.75	1.2	695	0	7.20	708.00	10.27	43.09	48.22
2	3.75	1.2	695	20	4.60	709.00	16.65	53.31	57.41
3	3.75	1.2	705	0	3.10	714.00	9.72	40.80	45.66
4	3.75	1.2	705	20	2.70	715.50	15.50	49.65	53.47
5	3.75	1.2	715	0	0.80	724.50	9.06	38.04	42.56
6	3.75	1.2	715	20	1.56	724.00	11.05	35.39	38.12
7	3.75	1.6	695	0	3.78	709.00	9.73	40.86	45.73
8	3.75	1.6	695	20	2.90	710.50	16.42	52.59	56.63
9	3.75	1.6	705	0	1.00	717.00	9.59	40.26	45.06
10	3.75	1.6	705	20	1.70	720.50	12.80	41.00	44.16
11	3.75	1.6	715	0	0.50	728.00	8.69	36.48	40.83
12	3.75	1.6	715	20	0.69	725.00	7.90	25.29	27.23
13	3.75	2	695	0	1.93	710.00	10.25	43.00	48.12
14	3.75	2	695	20	1.69	712.00	15.88	50.85	54.76
15	3.75	2	705	0	0.78	720.00	9.36	39.28	43.96
16	3.75	2	705	20	0.85	720.00	9.95	31.87	34.33
17	3.75	2	715	0	0.63	732.50	7.85	32.96	36.88
18	3.75	2	715	20	0.75	726.00	6.24	19.99	21.53
19	7.875	1.2	695	0	6.56	707.00	10.30	43.25	48.40
20	7.875	1.2	695	20	3.98	707.50	17.19	55.06	59.29
21	7.875	1.2	705	0	3.21	715.00	10.09	42.36	47.40
22	7.875	1.2	705	20	2.59	715.00	15.72	50.34	54.22
23	7.875	1.2	715	0	1.39	724.50	9.36	39.30	43.98
24	7.875	1.2	715	20	1.25	724.00	11.16	35.74	38.49
25	7.875	1.6	695	0	4.01	709.50	10.34	43.41	48.58
26	7.875	1.6	695	20	3.00	711.00	17.10	54.78	58.99
27	7.875	1.6	705	0	1.00	717.00	10.01	42.02	47.02
28	7.875	1.6	705	20	1.20	719.50	12.95	41.48	44.68
29	7.875	1.6	715	0	0.51	728.00	8.86	37.20	41.63
30	7.875	1.6	715	20	1.05	726.00	7.84	25.10	27.03
31	7.875	2	695	0	1.85	712.00	10.47	43.95	49.18
32	7.875	2	695	20	1.06	714.00	16.15	51.71	55.69
33	7.875	2	705	0	0.63	720.00	9.41	39.40	44.21
34	7.875	2	705	20	0.91	721.50	10.02	32.08	34.54
35	7.875	2	715	0	0.52	732.00	7.94	33.34	37.30
36	7.875	2	715	20	0.82	726.50	6.29	20.13	21.68
37	12	1.2	695	0	7.53	708.00	10.34	43.41	48.58
38	12	1.2	695	20	4.00	708.00	17.81	57.02	61.41
39	12	1.2	705	0	3.02	714.00	10.43	43.77	48.98
40	12	1.2	705	20	2.65	715.50	15.93	51.01	54.93
41	12	1.2	715	0	0.75	724.50	9.58	40.21	45.00
42	12	1.2	715	20	1.13	724.00	10.92	34.96	37.65
43	12	1.6	695	0	3.97	709.00	10.65	44.69	50.01
44	12	1.6	695	20	2.69	711.00	17.75	56.84	61.22
45	12	1.6	705	0	1.06	717.00	10.18	42.73	47.81
46	12	1.6	705	20	0.99	719.00	12.80	40.98	44.13
47	12	1.6	715	0	0.68	729.00	8.96	37.60	42.07
48	12	1.6	715	20	0.89	726.00	7.84	25.09	27.02
49	12	2	695	0	1.56	712.00	10.46	43.89	49.12
50	12	2	695	20	1.25	714.00	16.05	51.40	55.36

(*continued on next page*)

Table 1 (*continued*)

ID	Spray Cone Angle (degree)	Injection Duration (ms)	SOI (CA)	H_2 (%)	RI (MW/m^2)	PRA (CA)	IMEP (bar)	Exergy Efficiecy (%)	Energy Efficiency (%)
51	12	2	705	0	0.40	720.00	9.42	39.54	44.24
52	12	2	705	20	0.69	720.00	9.89	31.66	34.10
53	12	2	715	0	0.56	732.00	7.97	33.47	37.45
54	12	2	715	20	0.60	726.00	6.23	19.95	21.48
55	12	2	695	10	1.59	712.00	15.55	56.48	61.83
56	12	1.6	715	10	0.46	727.50	4.90	17.79	19.48
57	3.75	1.2	705	10	2.27	714.00	13.12	47.67	52.19
58	12	1.2	705	10	2.81	715.00	13.29	48.29	52.87
59	12	1.6	705	10	1.03	718.00	10.41	37.82	41.40
60	3.75	1.2	695	10	5.78	708.00	14.66	53.25	58.30
61	12	1.6	695	10	3.41	711.00	15.95	57.93	63.42
62	12	2	705	10	0.62	720.00	6.99	25.40	27.81
63	3.75	1.2	715	10	0.98	724.00	7.30	26.51	29.02
64	12	1.2	715	10	0.86	724.50	7.07	25.67	28.10
65	3.75	1.6	695	10	3.25	709.00	15.55	56.48	61.83
66	7.875	1.2	695	10	5.99	708.00	14.96	54.37	59.52
67	3.75	2	715	10	0.56	729.00	3.55	12.90	14.13
68	7.875	2	715	10	0.56	729.00	3.40	12.34	13.51
69	3.75	1.6	705	10	1.36	719.50	10.88	39.51	43.26
70	7.875	2	705	10	0.68	720.00	7.49	27.20	29.78
71	7.875	2	695	10	1.95	713.00	14.87	54.03	59.15
72	3.75	1.6	715	10	17.25	727.50	5.21	18.94	20.73
73	7.875	1.6	715	10	9.19	727.50	5.11	18.55	20.31
74	7.875	1.6	705	10	1.26	719.00	10.82	39.29	43.02
75	3.75	2	695	10	1.95	712.00	14.86	53.99	59.11
76	7.875	1.6	695	10	3.33	710.00	15.74	57.19	62.61
77	7.875	1.2	715	10	0.89	724.00	7.13	25.89	28.34
78	3.75	2	705	10	0.70	720.00	7.89	28.68	31.40
79	7.875	1.2	705	10	2.45	714.00	13.26	48.18	52.74
80	12	1.2	695	10	6.33	708.00	15.42	56.01	61.32
81	12	2	715	10	0.56	729.00	3.18	11.56	12.66
5 % H2-Premixed	7.5	1.2	712.5	5	1.35	720.00	11.09	44.07	46.73
Base Engine	7.5	1.35	712.5	0	0.55	720.00	8.88	37.08	41.63

Appendix II

$$\begin{aligned}\textbf{\textit{Exergy Efficiency}} = &-368.65+10.42(\textit{Spray Cone angle})+491.71(\text{Injection Duration})+0.58(\textit{SOI})+36.98(H_2\ \textit{Composition})\\&-0.20(\textit{Spray Cone angle}\times\text{Injection Duration})-0.01(\textit{Spray Cone angle}\times\text{SOI})\\&-0.0035(\textit{Spray Cone angle}\times H_2\ \textit{Composition})-0.7(\text{Injection Duration}\times\text{SOI})\\&-0.58(\text{Injection Duration}\times H_2\ \textit{Composition})-0.05(H_2\ \textit{Composition}\times\textit{SOI})\end{aligned}$$

$$\begin{aligned}\textbf{\textit{Energy Efficiency}} = &-400.21+11.40(\textit{Spray Cone angle})+537.92(\text{Injection Duration})+0.63(\textit{SOI})+39.65(H_2\ \textit{Composition})\\&-0.22(\textit{Spray Cone angle}\times\text{Injection Duration})-0.01(\textit{Spray Cone angle}\times\text{SOI})-0.004(\textit{Spray Cone angle}\\&\times H_2\ \textit{Composition})-0.76(\text{Injection Duration}\times\text{SOI})-0.61(\text{Injection Duration}\times H_2\ \textit{Composition})\\&-0.05(H_2\ \textit{Composition}\times\textit{SOI})\end{aligned}$$

$$\begin{aligned}\textbf{\textit{MPRR}} = &\,330.93+7.16(\textit{Spray Cone angle})-100.83(\text{Injection Duration})-0.44(\textit{SOI})-6.77(H_2\ \textit{Composition})\\&-0.01(\textit{Spray Cone angle}\times\text{Injection Duration})-0.01(\textit{Spray Cone angle}\times\text{SOI})-0.002(\textit{Spray Cone angle}\\&\times H_2\ \textit{Composition})+0.13(\text{Injection Duration}\times\text{SOI})+0.1(\text{Injection Duration}\times H_2\ \textit{Composition})\\&+0.009(H_2\ \textit{Composition}\times\textit{SOI})\end{aligned}$$

$$\begin{aligned}\textbf{\textit{PRA}} = &\,111.02+1.39(\textit{Spray Cone angle})-35.66(\text{Injection Duration})+0.84(\textit{SOI})+7.17(H_2\ \textit{Composition})\\&+0.04(\textit{Spray Cone angle}\times\text{Injection Duration})-0.002(\textit{Spray Cone angle}\times\text{SOI})-0.001(\textit{Spray Cone angle}\\&\times H_2\ \textit{Composition})+0.06(\text{Injection Duration}\times\text{SOI})-0.11(\text{Injection Duration}\times H_2\ \textit{Composition})\\&-0.009(H_2\ \textit{Composition}\times\textit{SOI})\end{aligned}$$

Data availability

Data will be made available on request.

References

[1] A. Jankowski, A. Sandel, J. Sęczyk, B. Siemińska-Jankowska, Some problems of improvement of fuel efficiency and emissions in internal combustion engines, Journal of KONES Internal Combustion Engines 9 (3–4) (2002) 333–356.
[2] X. Li, S. Yao, Z. Wang, X. Jiang, Y. Song, S.X. Chang, Polyethylene microplastic and biochar interactively affect the global warming potential of soil greenhouse gas emissions, Environmental Pollution (2022) 120433.
[3] A.S. Rajpoot, T. Choudhary, H.M. Chelladurai, G. Dwivedi, A novel comprehensive energy, exergy and sustainability analysis of a diesel engine powered by binary blends of juliflora biodiesel and nanoparticles, Journal of Thermal Analysis and Calorimetry 148 (21) (2023) 11981–11997.
[4] B. Shadidi, G. Najafi, T. Yusaf, A review of hydrogen as a fuel in internal combustion engines, Energies 14 (19) (2021) 6209.
[5] Y. Karagöz, İ. Güler, T. Sandalcı, L. Yüksek, A.S. Dalkılıç, Effect of hydrogen enrichment on combustion characteristics, emissions and performance of a diesel engine, Int. J. Hydrogen Energy 41 (1) (2016) 656–665.
[6] C. Deheri, S.K. Acharya, D.N. Thatoi, A.P. Mohanty, A review on performance of biogas and hydrogen on diesel engine in dual fuel mode, Fuel 260 (2020) 116337.
[7] H. Guo, W.S. Neill, The effect of hydrogen addition on combustion and emission characteristics of an n-heptane fuelled HCCI engine, Int. J. Hydrogen Energy 38 (26) (2013) 11429–11437.
[8] A.S. Rajpoot, T. Choudhary, H.M. Chelladurai, U. Rajak, A.A. Sinha, Effect of Oxy hydrogen (HHO) gas on energy, exergy, and sustainability analysis of a diesel engine fueled with palm oil biodiesel, Proc. Inst. Mech. Eng. Part E J. Process Mech. Eng. (2024) 09544089241259758.
[9] S. Gleis, S. Frankl, M. Prager, G. Wachtmeister, Optical analysis of the combustion of potential future E-Fuels with a high pressure dual fuel injection system, in: 14th International AVL Symposium on Propulsion Diagnostics, Baden Baden, 2020.
[10] Z. Li, Y. Wang, Z. Yin, Z. Gao, Y. Wang, X. Zhen, Parametric study of a single-channel diesel/methanol dual-fuel injector on a diesel engine fueled with directly injected methanol and pilot diesel, Fuel 302 (2021) 121156.
[11] M.A. Rosen, I. Dincer, Exergy as the confluence of energy, environment and sustainable development, Exergy An Int. J. 1 (1) (2001) 3–13.
[12] A. Bejan, Fundamentals of exergy analysis, entropy generation minimization, and the generation of flow architecture, Int. J. Energy Res. 26 (7) (2002).
[13] A.S. Rajpoot, T. Choudhary, H. Chelladurai, T.N. Verma, A. Pugazhendhi, Sustainability analysis of spirulina biodiesel and their blends on a diesel engine with energy, exergy and emission (3E's) parameters, Fuel 349 (2023) 128637.
[14] H. Taghavifar, A. Nemati, F.J. Salvador, J. De la Morena, 1D energy, exergy, and performance assessment of turbocharged diesel/hydrogen RCCI engine at different levels of diesel, hydrogen, compressor pressure ratio, and combustion duration, Int. J. Hydrogen Energy 46 (42) (2021) 22180–22194.
[15] T. Kraus, Hydrogen fuel–An economically viable future for the transportation industry, Duke Journal of Economics 19 (2007) 39.
[16] Y. Li, W. Gao, Y. Li, Z. Fu, J. Zou, Numerical investigation on combustion and knock formation mechanism of hydrogen direct injection engine, Fuel 316 (2022) 123302.
[17] H. Ge, A.H. Bakir, P. Zhao, Knock mitigation and power enhancement of hydrogen spark-ignition engine through ammonia blending, Machines 11 (6) (2023) 651.
[18] Z. Stępień, A comprehensive overview of hydrogen-fueled internal combustion engines: achievements and future challenges, Energies 14 (20) (2021) 6504.
[19] S. Verhelst, Recent progress in the use of hydrogen as a fuel for internal combustion engines, Int. J. Hydrogen Energy 39 (2) (2014) 1071–1085.
[20] M.D. Altinkurt, G. Coskun, M. Tunér, A. Turkcan, A comprehensive investigation of early pilot (e-pilot) mode split injection variations for improving NG-diesel dual-fuel combustion in a medium-speed marine engine: experiments and CFD study, Case Stud. Therm. Eng. 68 (2025) 105881.
[21] M. Steilen, L. Jörissen, Hydrogen conversion into electricity and thermal energy by fuel cells: use of H2-systems and batteries, in: Electrochemical Energy Storage for Renewable Sources and Grid Balancing, Elsevier, 2015, pp. 143–158.
[22] A. Lanz, J. Heffel, C. Messer, Hydrogen Fuel Cell Engines and Related Technologies," United States. Department of Transportation, Federal Transit Administration, 2001.
[23] H. Nazir, et al., Is the H2 economy realizable in the foreseeable future? Part II: H2 storage, transportation, and distribution, Int. J. Hydrogen Energy 45 (41) (2020) 20693–20708.
[24] A.Z. Ashkezari, A.H. Nezhad, S. Farahat, Reduction of pollutant emissions by developing a variable valve timing system in a direct injection diesel engine using computational fluid dynamics modeling, Environ. Prog. Sustain. Energy 35 (5) (2016) 1430–1440.
[25] S. Milojević, S. Savić, D. Marić, O. Stopka, B. Krstić, B. Stojanović, Correlation between emission and combustion characteristics with the compression ratio and fuel injection timing in tribologically optimized diesel engine, Teh. Vjesn. 29 (4) (2022) 1210–1219.
[26] M. Özkan, D.B. Özkan, O. Özener, H. Yılmaz, Experimental study on energy and exergy analyses of a diesel engine performed with multiple injection strategies: effect of pre-injection timing, Appl. Therm. Eng. 53 (1) (2013) 21–30.
[27] S.H. Park, I.M. Youn, C.S. Lee, Influence of ethanol blends on the combustion performance and exhaust emission characteristics of a four-cylinder diesel engine at various engine loads and injection timings, Fuel 90 (2) (2011) 748–755.
[28] B. Alizadeh Kharkeshi, R. Shafaghat, M. Mohebi, S. Talesh Amiri, M. Mehrabiyan, Numerical simulation of a heavy-duty diesel engine to evaluate the effect of fuel injection duration on engine performance and emission, Int. J. Eng. 34 (11) (2021) 2442–2451.
[29] J. Smits, Modeling of a Fluid Flow in an Internal Combustion Engine, Eindhoven University of Technology, 2006, pp. 1–97.
[30] M. Popovac, Robust eddy viscosity turbulence modeling with elliptic relaxation and compound wall treatment, Energies 16 (9) (2023) 3685.
[31] C.K. Law, Heat and mass transfer in combustion: fundamental concepts and analytical techniques, Progress in energy and combustion science 10 (3) (1984) 295–318.
[32] A. Rahimi, E. Fatehifar, R.K. Saray, Development of an optimized chemical kinetic mechanism for homogeneous charge compression ignition combustion of a fuel blend of n-heptane and natural gas using a genetic algorithm, Proc. Inst. Mech. Eng. - Part D J. Automob. Eng. 224 (9) (2010) 1141–1159.
[33] O. Vitek, V. Dolecek, D. Goryntsev, F. Tap, Z. Pavlovic, and P. Priesching, "Application of tabulated detailed chemistry to LES model of diesel ICE combustion," in *Internal Combustion Engine Division Fall Technical Conference*, 2019, vol. vol. 59346: American Society of Mechanical Engineers, p. V001T06A001.
[34] M. Tvrdojevic, P. Priesching, F. Tap, D. Goryntsev, Applying a Tabulated Chemistry Approach for the Calculation of Combustion and Emissions in Diesel Engines, 2017.
[35] Y.A. Cengel, M.A. Boles, M. Kanoğlu, Thermodynamics: an Engineering Approach, McGraw-hill, New York, 2011.
[36] J.A. Caton, Maximum efficiencies for internal combustion engines: thermodynamic limitations, Int. J. Engine Res. 19 (10) (2018) 1005–1023.
[37] M.J. Moran, H.N. Shapiro, D.D. Boettner, M.B. Bailey, Fundamentals of Engineering Thermodynamics, John Wiley & Sons, 2010.
[38] A. Ghannadzadeh, R. Thery-Hetreux, O. Baudouin, P. Baudet, P. Floquet, X. Joulia, General methodology for exergy balance in a process simulator, Computer Aided Chemical Engineering 29 (2011) 1758–1762. Elsevier.
[39] R. Pal, Chemical exergy of ideal and non-ideal gas mixtures and liquid solutions with applications, Int. J. Mech. Eng. Educ. 47 (1) (2019) 44–72.
[40] S. Jafarmadar, Exergy analysis of hydrogen/diesel combustion in a dual fuel engine using three-dimensional model, Int. J. Hydrogen Energy 39 (17) (2014) 9505–9514.
[41] J. Eng, Characterization of pressure waves in HCCI combustion. SAE Technical Paper, 0148-7191, 2002.
[42] P. Priesching, G. Ramusch, J. Ruetz, R. Tatschl, 3D-CFD modeling of conventional and alternative diesel combustion and pollutant formation-a validation study. SAE Technical Paper, 0148-7191, 2007.